SCIENTIFIC REPORTS

OPEN

SUBJECT AREAS:
ELECTRONIC STRUCTURE
SURFACES, INTERFACES AND THIN FILMS

Received
16 September 2014

Accepted
19 December 2014

Published
20 January 2015

Correspondence and requests for materials should be addressed to R.P. (Rossitza.Pentcheva@uni-due.de)

Control of orbital reconstruction in $(LaAlO_3)_M/(SrTiO_3)_N(001)$ quantum wells by strain and confinement

David Doennig[1] & Rossitza Pentcheva[1,2]

[1]Forschungs-Neutronenquelle Heinz Maier-Leibnitz (FRM II), Technische Universität München, Lichtenbergstraße 1, 85748 Garching, Germany, [2]Department of Physics and Center for Nanointegration Duisburg-Essen (CENIDE), University of Duisburg-Essen, Lotharstr. 1, 47057 Duisburg, Germany.

The diverse functionality emerging at oxide interfaces calls for a fundamental understanding of the mechanisms and control parameters of electronic reconstructions. Here, we explore the evolution of electronic phases in $(LaAlO_3)_M/(SrTiO_3)_N$ (001) superlattices as a function of strain and confinement of the $SrTiO_3$ quantum well. Density functional theory calculations including a Hubbard U term reveal a charge ordered Ti^{3+} and Ti^{4+} state for $N = 2$ with an unanticipated orbital reconstruction, displaying alternating d_{xz} and d_{yz} character at the Ti^{3+} sites, unlike the previously reported d_{xy} state, obtained only for reduced c-parameter at a_{STO}. At a_{LAO} c-compression leads to a Dimer-Mott insulator with alternating d_{xz}, d_{yz} sites and an almost zero band gap. Beyond a critical thickness of $N = 3$ (a_{STO}) and $N = 4$ (a_{LAO}) an insulator-to-metal transition takes place, where the extra $e/2$ electron at the interface is redistributed throughout the STO slab with a d_{xy} interface orbital occupation and a mixed $d_{xz} + d_{yz}$ occupation in the inner layers. Chemical variation of the $SrTiO_3$ counterpart ($LaAlO_3$ vs. $NdGaO_3$) proves that the significant octahedral tilts and distortions in the $SrTiO_3$ quantum well are induced primarily by the electrostatic doping at the polar interface and not by variation of the $SrTiO_3$ counterpart.

Oxide interfaces show surprisingly rich electronic behavior that is not present in the bulk compounds. Among the different systems, the (001)-oriented $LaAlO_3/SrTiO_3$ interface has been most prominent, displaying two-dimensional conductivity, superconductivity and magnetism, as well as confinement-induced metal-to-insulator transitions[1–5]. The majority of experimental studies have explored thin $LaAlO_3$ (LAO)-films on $SrTiO_3$ (001). In contrast, superlattices containing two n-type interfaces with a LaO and TiO_2 stacking have been in the focus of theoretical studies[6–10]. The latter predict that the excess charge of $0.5e$ at the polar interface results either in a charge ordered phase with d_{xy} orbital polarization or a quasi two-dimensional electron gas (2DEG) where the excess charge of $0.5e$ is delocalized throughout the $SrTiO_3$ (STO) quantum well. While the experimental realization of this type of superlattice remains a challenge as it requires precise control of termination at both interfaces, there is renewed interest in such systems in view of confinement effects in electrostatically doped oxide quantum wells. To this end, recent experimental studies on related $GdTiO_3/SrTiO_3$ superlattices by Moetakef *et al.*[11] reported the formation of a high density 2DEG where the carrier concentration can be modulated by the thickness of the STO quantum well. Moreover, a metal-to-insulator transition and ferromagnetism is induced for STO thickness below two unit cells (containing two SrO layers)[12]. In contrast, the analogous $SmTiO_3/SrTiO_3$ superlattice (SL) remains metallic down to a single SrO layer[13]. This distinct behavior of the two systems has been related to differences in octahedral tilts and distortions, induced by $GdTiO_3$ or $SmTiO_3$.

These findings have motivated us to revisit the LAO/STO superlattices and explore systematically the types of electronic and orbital reconstructions that can be realized as a function of STO confinement. We note that LAO/STO SLs have the advantage that the transition metal ion is only confined to the STO part, therefore emerging effects, including magnetism can be unambiguously associated with the STO quantum well (QW). We relate the electronic behavior to the structural changes by fully considering octahedral tilts and distortions as well as the role of the vertical lattice parameter. We note that previous work[6,7] has addressed predominantly tetragonally distorted superlattices, where due to symmetry restrictions, only a structural optimization of the z position of the ions was performed. $GdFeO_3$-type distortions have been considered by Zhong and Kelly[8] only for a $(LAO)_M/$

$(STO)_N$ (001) superlattices with $N = 3$. Here, we have investigated the behavior as a function of N. In particular, a critical thickness for a metal-to-insulator transition in this system is determined.

Strain is a powerful tool to tune the electronic behavior and orbital polarizations[14,15], but so far only a few studies have addressed this effect in the LAO/STO system. Bark *et al.*[16] studied its influence on the properties of $LaAlO_3$ films on $SrTiO_3$ (001) by growing the system on substrates with different lattice parameters. Transport measurements show that under compressive strain the 2DEG is preserved, but with reduced carrier concentration compared to the system grown on $SrTiO_3$(001), whereas for larger tensile strain the 2DEG is quenched. Furthermore, recent experiments have shown variations of carrier density and mobility of the 2DEG when exchanging $LaAlO_3$ by other polar RBO_3 oxides (R = La, Pr, or Nd, B = Al or Ga)[17].

The goal of this theoretical study is to explore systematically the influence of strain, confinement and chemical variation on the electronic and orbital reconstruction in (001)-oriented $(LAO)_M/(STO)_N$ superlattices, where N is varied between 2–4. Octahedral tilts and distortions, considered to be an important factor in tuning the properties of the 2DEG at these oxide interfaces, were fully taken into account. Additionally, we also performed optimization of the out-of-plane lattice parameter c. The effect of chemical control on the interface properties is addressed by replacing the polar $LaAlO_3$ with the polar $NdGaO_3$(NGO).

Results

Electronic and orbital reconstruction $(LAO)_M/(STO)_N$(001) SLs: influence of strain. *Results for a_{STO}, corresponding to an underlying STO(001) substrate.* Figure 1 presents results for n-type (001)-oriented $(LAO)_M/(STO)_N$ superlattices with varying thickness of the STO quantum well, N = 2–4. Using the c parameter that corresponds to volume conservation of the corresponding bulk constituents, the $SrTiO_3$ bilayer ($N = 2$ case) under tensile strain (a_{STO}) [Fig. 1(a)] is a charge-ordered ferromagnetic insulator with alternating Ti^{3+} (0.59 μ_B) and Ti^{4+} (0.11 μ_B) sites with a d_{xy} orbital occupation at the Ti^{3+} sites, consistent with previous work[6–8]. Surprisingly, for the optimized c parameter of 3.87 Å (0.23 Å larger) the charge-ordered pattern is preserved, however the orbital order at the Ti^{3+} sites changes to d_{xz} for Ti^{3+} at the top interface and d_{yz} for Ti^{3+} at the bottom interface [Fig. 1(b)]. This is associated with a much narrower occupied Ti 3d band and an enhanced effective mass of 3.57 m_e, indicating an increase of electron correlation effects. Simultaneously the size of the band gap is enlarged from 0.16 eV to 0.42 eV. The magnetic moment of the Ti^{3+} sites increases slightly from 0.59 μ_B to 0.64 μ_B.

The mechanism of electronic reconstruction is distinct for the thicker STO quantum wells, N = 3 [Fig. 1(c)] and N = 4 [Fig. 1(d)]. Here, the extra $e/2$ charge from each interface is redistributed throughout the STO slab, resulting in an insulator-to-metal transition with a critical thickness $N_c = 3$. In both cases the charge-ordered state is suppressed. Simultaneously, the orbital polarization is altered to predominantly d_{xy} orbital character in the interface Ti-layer and mixed $d_{xz} + d_{yz}$ in the central Ti layers, similar to previous findings in $(LAO)_M/(STO)_N$ superlattices[7,9,10,18].

Results for a_{LAO}, corresponding to an underlying LAO(001) substrate. Figure 2 shows the results for (001)-oriented $(LAO)_M/(STO)_N$ heterostructures with STO thickness ranging from N = 2–4. For the $SrTiO_3$ bilayer ($N = 2$) the ground state under compressive strain (a_{LAO}) and optimized c parameter [see Fig. 2(b)] is analogous to the one for a_{STO} [cf. Fig. 1(b)]: a charge-ordered insulating phase with Ti^{3+} and Ti^{4+} in a checkerboard arrangement and a d_{xz}, d_{yz} orbital polarization at the Ti^{3+} sites at each interface, albeit with slightly smaller magnetic moment (0.61 μ_B) at the Ti^{3+} sites. This is accompanied by an increase of the band gap from 0.42 eV (a_{STO}) to 0.65 eV (a_{LAO}).

An interesting electronic state occurs for $N = 2$ upon compression of the c parameter of the superlattice to the bulk LAO value [see Fig. 2(a)]: The charge-ordered state is quenched, leaving 0.5e at each Ti site (0.33 μ_B) and alternating d_{xz}, d_{yz} orbital polarization on neighboring Ti sites in a checkerboard arrangement. Characteristic for this

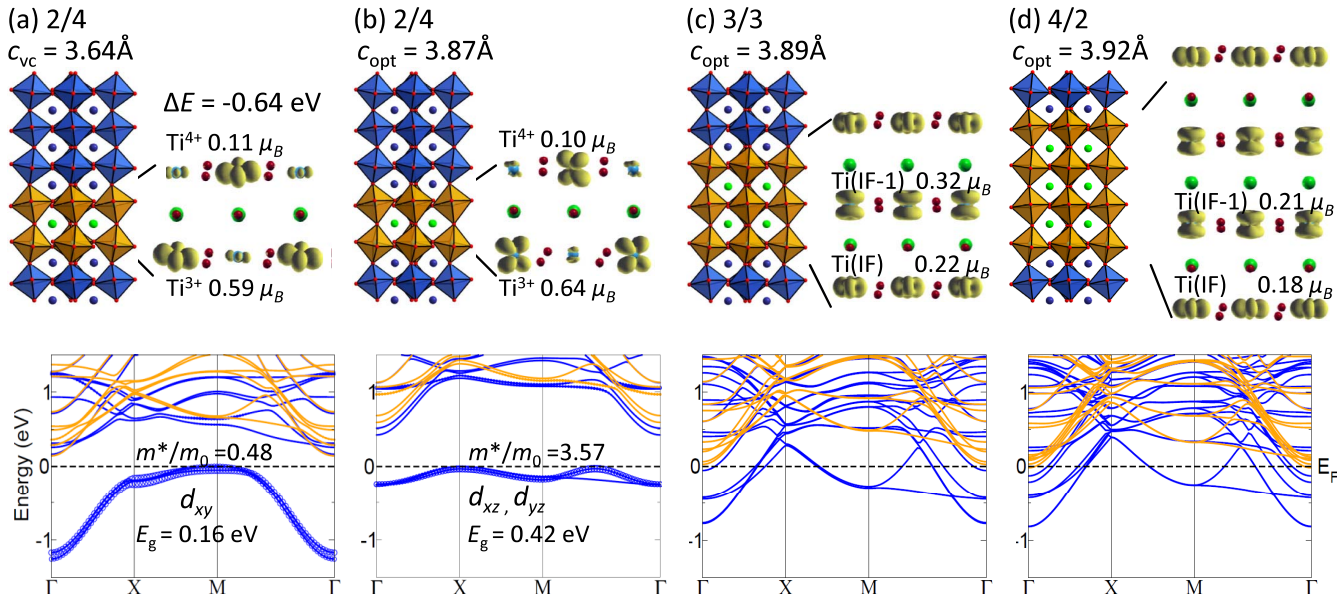

Figure 1 | Side view of the relaxed structure, electron density distribution, integrated over occupied Ti 3d bands between E_F-1.5 eV and E_F and band structure in $(LAO)_M/(STO)_N$ (001) SL at a_{STO}. Majority and minority bands are plotted in blue and orange, respectively. Character plotting highlights the occupied d band at the Ti^{3+} sites. (a) $N = 2$ is a charge-ordered FM insulator with d_{xy} orbital occupation at the Ti^{3+} sites for the c-parameter fixed to conserve the volume and (b) with d_{xz} and d_{yz} orbital occupation at Ti^{3+} at each interface layer for the optimized c-parameter. ΔE is the energy difference (in eV per Ti site) between the cases shown in (b) and (a); (c)–(d) For $N = 3, 4$ STO layers, the charge-ordered state is suppressed and the system switches from insulating to conducting behavior with a d_{xy} orbital at the Ti interface sites and $d_{xz} + d_{yz}$ orbital occupation in the central STO layers.

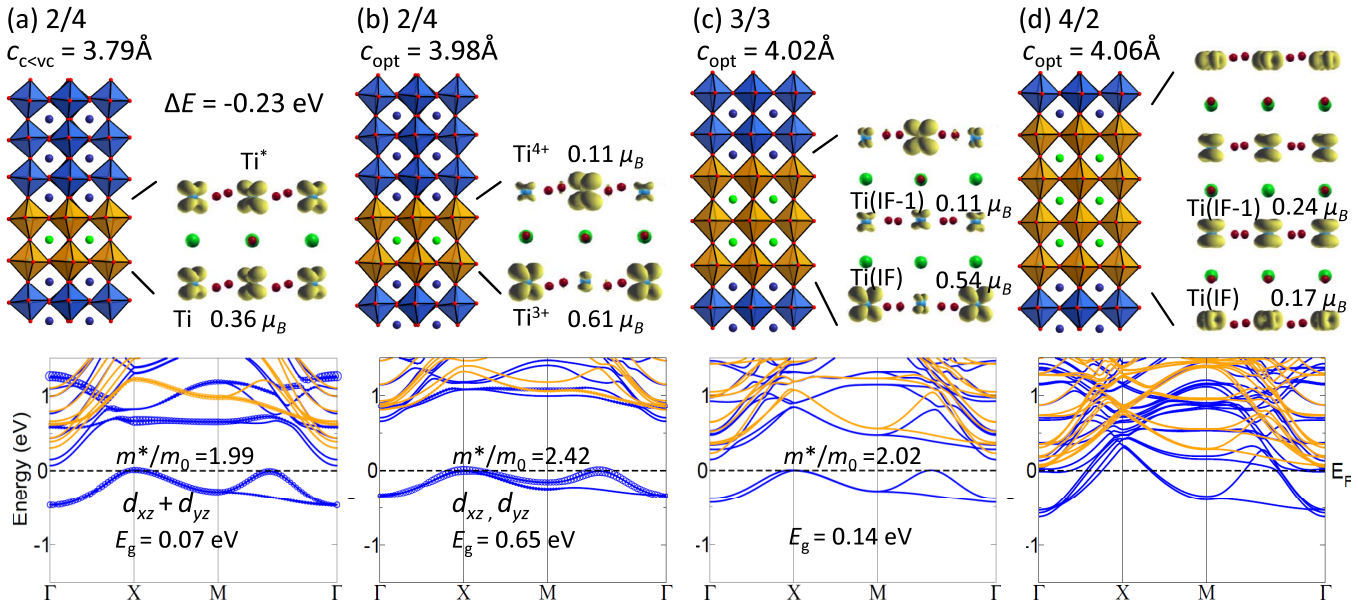

Figure 2 | Side view of the relaxed structure, electron density distribution, integrated over occupied Ti 3*d* bands between E_F-1.5 eV and E_F, and band structure of $(LAO)_M/(STO)_N$ (001) SL at a_{LAO}, N = 2–4. Majority and minority bands are plotted in blue and orange, respectively. Character plotting highlights the occupied *d* band at the Ti^{3+} sites. (a) For $N = 2$ a Dimer Mott insulator is obtained for the strongly compressed *c* parameter with alternating d_{xz}, d_{yz} orbital occupation at the $Ti^{3.5+}$ sites; (b) for the optimized *c* a charge ordered state with d_{xz} and d_{yz} orbital occupation at the Ti^{3+} sites at each interface layer emerges; ΔE is the energy difference (in eV per Ti site) between the cases shown in (b) and (a); (c) $N = 3$ is similar to (b) with Ti^{4+} in the central layer; (d) an insulator to metal transition takes place for $N = 4$: with a d_{xy} orbital polarization at the Ti interface sites and $d_{xz} + d_{yz}$ orbital occupation in the inner STO layers.

state is a decreased but nonzero band gap (0.07 eV). This so called Dimer Mott insulator (DMI), initially predicted within the framework of one-dimensional Hubbard ladders[19], was recently suggested for GTO/STO QWs for a single SrO layer in a $GdTiO_3$ matrix[20]. In fact the ground state for the optimized *c*-value can be regarded as emerging from the DMI phase by transferring 0.5*e* between each pair of Ti sites, leading to a Ti^{3+} and Ti^{4+} charge order with some residual d_{xz} orbital occupation at the Ti^{4+} sites and d_{yz} at the Ti^{3+} sites at one interface and the opposite orbital polarization in the other interface layer.

To explore how the combination of exchange correlation functional (LDA vs GGA) and the Coulomb repulsion term influence the structural properties and electronic ground state, we have performed additional calculations for $(LAO)_4/(STO)_2(001)$ at a_{LAO}, using the LDA + *U* functional. Setting the lateral lattice parameter to the experimental bulk LAO value of 3.79 Å, the optimized *c* lattice parameter (3.83 Å) is ~4% smaller than the GGA + *U* value (3.98 Å). The electronic ground state in Fig. 2(b) with Ti^{3+} and Ti^{4+} in a checkerboard arrangement and a d_{xz}, d_{yz} orbital polarization at the Ti^{3+} sites emerges within LDA + *U* beyond $U = 5.5$ eV. Thus we can conclude that the electronic ground state is largely unaffected by the reduction of the *c*-lattice parameter within LDA + *U* and is stabilized for a slightly higher value of *U* than in the GGA + *U* calculation.

Unlike the corresponding case at a_{STO}, the electronic and orbital reconstruction persists for $N = 3$ [see Fig. 2(c)] i.e. a charge-ordered state with alternating d_{xz}, d_{yz} at the Ti^{3+} sites emerges at both interface layers, whereas the central layer becomes Ti^{4+}. Compared to the case with $N = 2$ with optimized *c*, the band width is increased and the band gap is reduced to 0.14 eV. The magnetic moment at the Ti^{3+} sites is reduced to (0.54 μ_B), indicating an enhanced delocalization.

An insulator-to-metal transition takes place at a STO thickness $N = 4$ [see Fig. 2(d)]. The suppression of the charge ordered state leads to a closing of the band gap. The extra *e*/2 charge is delocalized throughout the whole STO quantum well with a preferential d_{xy} orbital occupation at the interface layer and a $d_{xz} + d_{yz}$ occupation in the central layers.

Structural relaxations. To investigate the relationship between electronic properties and structural distortions we have performed a quantitative analysis of the fully relaxed $(LAO)_M/(STO)_N$ (001) superlattices. The B-O-B bond angles in the perovskite structure ABO_3 are closely related to octahedral tilts and determine orbital overlaps, and are therefore considered to be the control parameter

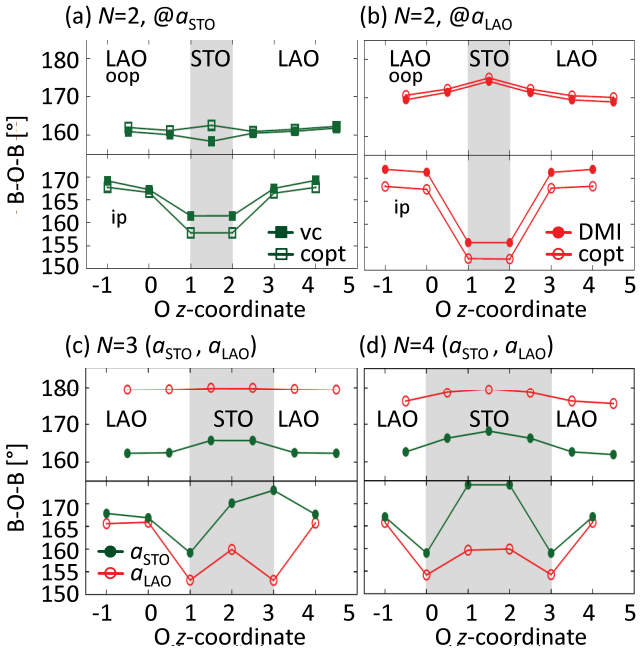

Figure 3 | Quantitative analysis of B-O-B bond angles in $(LAO)_M/(STO)_N$ (001) superlattices for different STO thicknesses *N* (shaded region). (a) The bilayer $N = 2$ under tensile strain (a_{STO}). (b) STO bilayer for compressive strain (a_{LAO}). (c)–(d) $N = 3$, 4 STO layers.

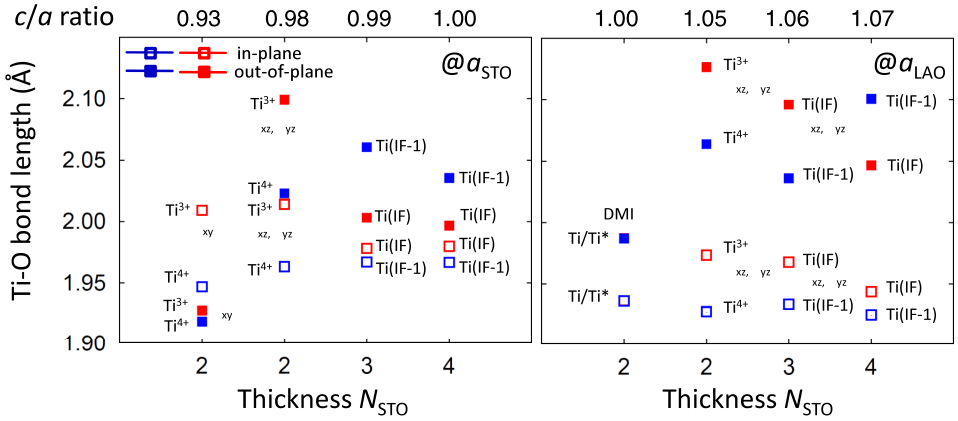

Figure 4 | In-plane (hollow squares) and out-of-plane (solid squares) Ti-O bond lengths for the distinct Ti sites in $(LAO)_M/(STO)_N$ (001) superlattices at a_{STO} (left panel) and a_{LAO} (right panel). The corresponding c/a ratio is given at the top of the graphs.

for metal-to-insulator transitions in bulk transition metal oxides[21,22]. Understanding the origin of modifications of octahedral tilts and connectivity at interfaces in oxide superlattices is an emerging topic of considerable interest[14,23].

In Fig. 3 we present the B-O-B bond angles of the superlattices as a function of the inplane lattice constant a_{STO} and a_{LAO}. The corresponding results for a_{NGO} are displayed in Fig. 5. In the $(LAO)_M/(STO)_N$ (001) superlattices we identify strong reduction of the B-O-B angles from the bulk values. We remind that bulk $SrTiO_3$ has the ideal cubic perovskite structure ($Pm\bar{3}m$) with B-O-B bond angles of 180°. Below 105 K it undergoes an antiferrodistortive phase transition to a tetragonal ($I4/mcm$) structure[24], whereas $LaAlO_3$ attains a rhombohedral structure ($R\bar{3}c$) at all temperatures with B-O-B bond angles of 171.4°. As shown in Fig. 3 and 5, the deviations of the B-O-B bond angles from the ideal 180° are most prominent in the STO quantum well. Moreover, there are pronounced differences in the behavior of in-plane and out-of-plane angles and their strain dependence: For all studied thicknesses of the STO quantum well (N = 2–4), the in-plane B-O-B bond angles show the strongest deviation from 180° in particular in the STO part, while in the LAO part the deviations of the bond angles are smaller and converge towards the bulk LAO value away from the interface. As a function of strain, the ones in the STO part (N = 2) increase with the lateral lattice constant, i.e. ~152° at a_{LAO}, followed by ~155° at a_{NGO} and finally ~158° at a_{STO}. The opposite trend is observed for the out-of-plane BOB bond angles. Here the strongest deviation from 180° is for a_{STO} (~162°), then a_{NGO} (~168°) and lowest for a_{LAO} (~175°). Moreover, the variation in out-of-plane bond angles between the LAO and STO part of the SL is much weaker than the in-plane bond angles.

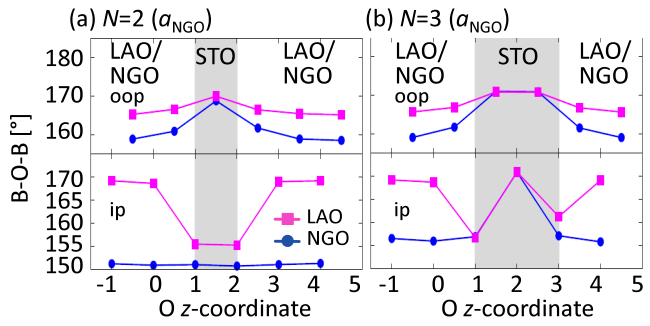

Figure 5 | Quantitative analysis of B-O-B bond angles in (001)-oriented $(LAO)_M/(STO)_N$ and $(NGO)_M/(STO)_N$ superlattices with the in-plane lattice parameter fixed at a_{NGO} for different STO thicknesses N (shaded region). (a) N = 2 STO layers. (b) N = 3 STO layers.

In order to relate the structural distortions to the resulting orbital reconstruction, in Fig. 4 we have also analyzed the corresponding Ti-O bond lengths. N = 2 under tensile strain with c-parameter fixed to conserve the volume comprises the only case where the in-plane bond distance is larger than the out-of-plane Ti-O length. This is consistent with the d_{xy} orbital order at Ti^{3+}. For all other cases, the out-of-plane Ti-O bond distance is larger than the in-plane value. These differences are particularly pronounced at the Ti^{3+} sites, e.g. 2.10 vs. 2.01 Å at a_{STO} and 2.13 vs. 1.97 at a_{LAO} for N = 2, respectively. A similar trend but with smaller absolute values is observed at the Ti^{4+} sites (2.02 vs. 1.96 Å and 2.06 vs. 1.93 Å, respectively). The enhanced out-of-plane to in-plane distance ratio favors the alternating d_{xz}, d_{yz} orbital polarization. As this trend is stronger for a_{LAO}, it is responsible for the stabilization of this orbital order and consequently the insulating state up to N = 3, while at a_{STO} the system is already metallic for N = 3. As discussed above, the insulator-to-metal transition is connected with a change in orbital polarization to d_{xy} in the interface layer and mixed $d_{xz}+d_{yz}$ in the inner layer. Indeed the difference in out-of-plane to in-plane distance is reduced (a_{LAO}: 2.06 vs. 1.93 Å) and almost quenched at Ti(IF) (a_{STO}: 2.00 vs 1.98 Å) for

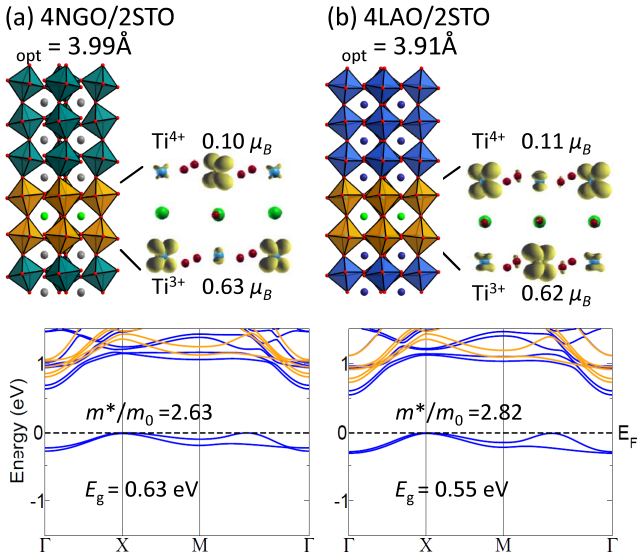

Figure 6 | Side view of the relaxed structure, electron density distribution, integrated over occupied Ti 3d bands between E_F-1.5 eV and E_F and band structure in (001)-oriented $(NGO)_M/(STO)_N$ and $(LAO)_M/(STO)_N$ superlattices at a_{NGO} with N = 2. Majority and minority bands are plotted in blue and orange, respectively.

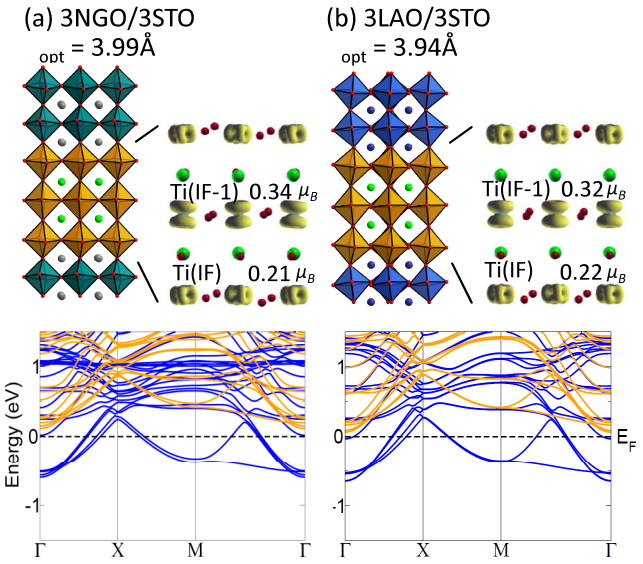

Figure 7 | Side view of the relaxed structure, electron density distribution, integrated over occupied Ti 3*d* bands and band structure in (001)-oriented $(NGO)_M/(STO)_N$ and $(LAO)_M/(STO)_N$ superlattices at a_{NGO} with $N = 3$. Majority and minority bands are plotted in blue and orange, respectively.

$N = 4$. Conversely, the inner (IF-1) layers show a larger difference (a_{LAO}: 2.10 vs. 1.92 Å; a_{STO}: 2.03 vs. 1.97 Å). Thus changes in the in-plane and out-of-plane bond lengths clearly reflect the trends in orbital polarization as a function of strain and thickness N of the STO quantum well.

Chemical control: $(LAO)_M/(STO)_N(001)$ vs. $(NGO)_M/(STO)_N(001)$. To explore how chemical variation of the STO counterpart influences the electronic reconstruction and relaxations in the STO QW, we performed calculations on *n*-type $(NGO)_M/(STO)_N$ (001) superlattices with the in-plane lattice parameter fixed to a_{NGO}, which formally has the same polar discontinuity across the interface. For comparison, Figs. 5, 6 and 7 contain also the structural and electronic properties $(LAO)_M/(STO)_N$ (001) superlattices at a_{NGO}.

Fig. 5 compares the evolution of in-plane and out-of-plane B-O-B bond angles across the interface, for the $NdGaO_3/SrTiO_3$ and $LaAlO_3/SrTiO_3$ superlattices with $N = 2$, 3. For $N = 2$ (see Fig. 5(a)), the in-plane bond angle in the $NdGaO_3/SrTiO_3$ heterostructure remains nearly constant (~151°) throughout the superlattice. This value is slightly smaller but close to the bulk value (153.2°) of orthorhombic NGO (*Pbnm*). For the $LaAlO_3/SrTiO_3$ superlattice the bond angle in the STO quantum well is strongly reduced from the bulk STO value to ~155°. Moving away from the interface into the LAO part, the B-O-B bond angles quickly approach the LAO bulk value of 171.4°. In contrast, for both superlattices, the out-of-plane bond angle deviations 180° in the STO part are less pronounced and the values almost coincide for the $NdGaO_3/SrTiO_3$ and the $LaAlO_3/SrTiO_3$ superlattices in the center of the STO part, whereas they converge towards the NGO and LAO bulk values outside the STO QW.

Increasing the STO thickness to $N = 3$ (see Fig. 5(b)), the in-plane bond angle deviations are significantly reduced in the central STO part (~170°), but are still quite prominent at the interface (~157°). The deviation of the out-of-plane bond angles is similar as for the superlattices with $N = 2$.

The similarity in structural relaxation of the $NdGaO_3/SrTiO_3$ and the $LaAlO_3/SrTiO_3$ superlattices goes hand in hand with common electronic properties: For $N = 2$, the ground state for both systems is an insulating charge-ordered phase with Ti^{3+} and Ti^{4+} sites (see Fig. 6). Increasing the STO thickness to $N = 3$, the system undergoes an insulator-to-metal transition (see Fig. 7). The charge-ordered state is suppressed and the excess charge is delocalized throughout the STO slab, similar to the corresponding case at a_{STO} (see Fig. 1(c)).

Discussion

A central question is the origin of the unanticipated orbital reconstruction and how it relates to the STO QW thickness and structural distortions. Our results suggest that the electronic ground state and orbital polarization are intimately related to the level of electrostatic doping of the system. By construction the polar discontinuity at the interface introduces 0.5*e* per lateral unit cell at each interface, corresponding to a carrier density of $\sim 7 \times 10^{14}$ cm^{-2}. $N = 2$ comprises an extreme case with doping of 0.5*e* per Ti site. With increasing N_{STO} the excess charge is redistributed throughout the STO QW, resulting in a reduction of the carrier density and the effective filling of the Ti 3*d* band. We consider this reduction of carrier density with increasing N_{STO} as the driving force for the switching of orbital polarization from d_{xz}, d_{yz} at the Ti^{3+} sites for $N = 2$ to d_{xy} in the interface layer and mixed d_{xz}, d_{yz} in the inner layers beyond $N = 3$ as well as for the concomitant insulator-to-insulator transition.

It is instructive to compare the LAO/STO SLs to GTO/STO system[11]. For the latter a similar critical thickness of $N = 3$ was reported for the insulator-to-metal transition. In both cases the QW thickness reduction increases the effective carrier density and brings the system into a state where the on-site Coulomb repulsion becomes relevant, as pointed out by Ouellette *et al.*[25].

Concerning the orbital reconstruction most of previous studies have reported a dominant d_{xy} orbital polarization[6,7,18]. Here we find that this orbital polarization is stabilized only for a compressed *c* lattice parameter, whereas the ground state comprises a d_{xz}, d_{yz} ordering at the Ti^{3+} sites. Beyond the critical thickness, a crossover to a d_{xy} character in the interface layer and a mixed d_{xz}, d_{yz} character in the inner layers takes place. This is consistent with recent finding of a dominant contribution of d_{xz}, d_{yz} orbitals to the Fermi surface in LAO/STO, where doping levels beyond $\sim 6.9 \times 10^{14}$ cm^{-2} were achieved through oxygen vacancy doping[26]. The origin of orbital polarization and insulator-to-metal transition is further substantiated by the analysis of bond lengths (see. Fig. 4). The d_{xz}, d_{yz} orbital polarization at the Ti^{3+} sites is associated with significant elongation of the octahedra, whereas the transition from insulating-to-metallic state at the critical STO thickness is reflected in a reduction/increase in the apical to basal bond length ratio in the IF/IF-1 layer.

A key structural feature are the strong tilts of the TiO_6 octahedra, in particular at the interface, in contrast to the undistorted bulk STO. In the related GTO/STO superlattices[11] this behavior was ascribed to the influence of GTO, which has bulk B-O-B angles of 155°. As LAO has a much larger B-O-B angle of 171.4°, we can unambiguously conclude that the B-O-B angle reduction in the STO QW is not induced by the STO counterpart LAO, but correlates with the Ti 3*d* band occupation and the localization of charge. This is furthermore confirmed by the similar structural and electronic behavior of the STO QW in the $NdGaO_3/SrTiO_3$ (bulk NGO has B-O-B angles of 153°) and the $LaAlO_3/SrTiO_3$ superlattices. In particular, the strongest changes in the in-plane B-O-B angles are observed at the interface at Ti^{3+} sites, whereas the changes are much smaller and even quenched in the inner layers or at Ti^{4+} sites, as can be observed for $N = 3$ and 4 in Figs. 3c and d.

In summary, DFT+*U* calculations, performed on (001)-oriented $(LAO)_M/(STO)_N$ and $(NGO)_M/(STO)_N$ superlattices with *n*-type interfaces show a rich set of orbital reconstructions depending on the STO quantum well thickness and *c*/*a* ratio. For $N = 2$ the ground state is a charge ordered Ti^{3+}, Ti^{4+} phase characterized by unanticipated d_{xz}, d_{yz} orbital polarization and elongated Ti^{3+}-O_6 octahedra. *c* lattice compression leads to a Dimer Mott insulator (a_{LAO}) or a d_{xy} orbital polarization (a_{STO}), the latter case being the only one with

compressed Ti^{3+}-O_6 octahedra. With increasing STO quantum well thickness an insulator-to-metal transition takes place. The changes in the in-plane to out-of-plane bond length ratios signal the switching of orbital polarization and the critical thickness for the insulator-to-metal transition. A central finding is the pronounced enhancement of octahedral tilts in the STO quantum well that are not present in the bulk and can be unambiguously associated with the electrostatic doping of the polar *n*-type interface in these systems. Together with the exotic electronic states found in (111)-oriented $(LAO)_M/(STO)_N$ SLs[27], the results demonstrate how strain and the thickness of the STO quantum well can be used to engineer the orbital reconstruction and insulator-to-metal transitions in oxide superlattices.

Such an emergence of strong octahedral tilts associated with a transition to a Mott insulating phase were recently predicted also in doped bulk $SrTiO_3$[35].

Methods

DFT calculations were performed on *n*-type $(LAO)_M/(STO)_N(001)$ and $(NGO)_M/(STO)_N$ (001) superlattices with varying thickness *M*, *N* of the constituents, using the all-electron full-potential linearized augmented-plane-wave (LAPW) method, as implemented in the WIEN2k code[28]. For the exchange-correlation functional we used the generalized gradient approximation (GGA)[29]. Static local electronic correlations were taken into account in the GGA + *U* method[30] with $U = 5$ eV, $J = 0.7$ eV (Ti 3*d*), $U = 8$ eV (La 4*f*, Nd 4*f*). For oxides containing Ti^{3+} ($3d^1$) values between $U = 3$–8 eV have been used in previous studies[6–8,31–33]. The influence of strain was explored by setting the lateral lattice parameter to the one of LAO ($a_{LAO} = 3.79$Å), NGO ($a_{NGO} = 3.86$Å) or STO ($a_{STO}^{GGA} = 3.92$Å), corresponding to superlattices grown on the respective (001) substrate. Octahedral tilts and distortions were fully considered by relaxing atomic positions in P1 symmetry using a $\sqrt{2}a \times \sqrt{2}a$ lateral unit cell. Additionally the out-of-plane lattice parameter *c* was optimized for all superlattices. The effective masses of the electrons were calculated by fitting the region around the Gamma point to a quadratic polynomial. Isosurface plots of the electron density were generated by XCrySDen, written by A. Kokalj[34].

1. Ohtomo, A. & Hwang, H. Y. A high-mobility electron gas at the $LaAlO_3/SrTiO_3$ heterointerface. *Nature* **427**, 423 (2004).
2. Reyren, N. *et al.* Superconducting interfaces between insulating oxides. *Science* **317**, 1196 (2007).
3. Brinkman, A. *et al.* Magnetic effects at the interface between non-magnetic oxides. *Nat. Mater.* **6**, 493 (2007).
4. Hwang, H. Y. *et al.* Emergent phenomena at oxide interfaces. *Nat. Mater.* **11**, 103–113 (2012).
5. Thiel, S. *et al.* Tunable quasi-two-dimensional electron gases in oxide heterostructures. *Science* **313**, 1942–1945 (2006).
6. Pentcheva, R. & Pickett, W. E. Charge localization or itineracy at $LaAlO_3/SrTiO_3$ interfaces: Hole polarons, oxygen vacancies, and mobile electrons. *Phys. Rev. B* **74**, 035112 (2006).
7. Pentcheva, R. & Pickett, W. E. Ionic relaxation contribution to the electronic reconstruction at the *n*-type $LaAlO_3/SrTiO_3$ interface. *Phys. Rev. B* **78**, 205106 (2008).
8. Zhong, Z. & Kelly, P. J. Electronic-structure-induced reconstruction and magnetic ordering at the $LaAlO_3/SrTiO_3$ interface. *Europhys. Lett.* **84**, 27001 (2008).
9. Popovic, Z. S., Satpathy, S. & Martin, R. M. Origin of the Two-Dimensional Electron Gas Carrier Density at the $LaAlO_3$ on $SrTiO_3$ Interface. *Phys. Rev. Lett.* **101**, 256801 (2008).
10. Janicka, K. Velev, J. P. & Tsymbal, E. Magnetism of $LaAlO_3/SrTiO_3$ superlattices. *J. Appl. Phys.* **103**, 07B508 (2008).
11. Moetakef, P. *et al.* Toward an artificial Mott insulator: Correlations in confined high-density electron liquids in $SrTiO_3$. *Phys. Rev. B* **86**, 201102(R) (2012).
12. Moetakef, P. *et al.* Carrier-Controlled Ferromagnetism in $SrTiO_3$. *Phys. Rev. X* **2**, 021014 (2012).
13. Zhang, J. Y. *et al.* Correlation between metal-insulator transitions and structural distortions in high-electron-density $SrTiO_3$ quantum wells. *Phys. Rev. B* **89**, 075140 (2014).
14. Rondinelli, J. M., May, S. J. & and Freeland, J. W. Control of octahedral connectivity in perovskite oxide heterostructures: An emerging route to multifunctional materials discovery. *MRS Bulletin* **37**, 261 (2012).
15. Schlom, D. G. *et al.* Elastic strain engineering of ferroic oxides. *MRS Bulletin* **39**, 118–130 (2014).
16. Bark, C. W. *et al.* Tailoring a two-dimensional electron gas at the $LaAlO_3/SrTiO_3$ (001) interface by epitaxial strain. *Proc. Natl. Acad. Sci. USA* **108**, 4720 (2011).
17. Annadi, A. *et al.* Electronic correlation and strain effects at the interfaces between polar and nonpolar complex oxides. *Phys. Rev. B* **86**, 085450 (2012).
18. Salluzzo, M. *et al.* Orbital Reconstruction and the Two-Dimensional Electron Gas at the $LaAlO_3/SrTiO_3$ Interface. *Phys. Rev. Lett.* **102**, 166804 (2009).
19. Dagotto, E. & Rice, T. M. Surprises on the Way from One- to Two-Dimensional Quantum Magnets: The Ladder Materials. *Science* **271**, 618–623 (1996).
20. Chen, R., Lee, S. & Balents, L. Dimer Mott insulator in an oxide heterostructure. *Phys. Rev. B* **87**, 161119(R) (2013).
21. Goodenough, J. B. & Zhou, J. S. Orbital ordering in orthorhombic perovskites. *J. Mater. Chem.* **17**, 2394–2405 (2007).
22. Medarde, M. L. Structural, magnetic and electronic properties of $RNiO_3$ perovskites (R = rare earth). *J. Phys.: Condens. Matter* **9**, 1679 (1997).
23. Rondinelli, J. M. & Spaldin, N. A. Structure and Properties of Functional Oxide Thin Films: Insights From Electronic-Structure Calculations. *Adv. Mater.* **23**, 3363 (2011).
24. Müller, K. A. & Burkhard, H. $SrTiO_3$: An intrinsic quantum paraelectric below 4 K. *Phys. Rev. B* **19**, 3593 (1979).
25. Ouellette, D. G. *et al.* High-density two-dimensional small polaron gas in a delta-doped Mott insulator. *Sci. Rep.* **3**, 3284 (2013).
26. Petrovic, A. P. *et al.* Long-range electronic reconstruction to a $d_{xz,\ yz}$-dominated Fermi surface below the $LaAlO_3/SrTiO_3$ interface. *Sci. Rep.* **4**, 5338 (2014).
27. Doennig, D., Pickett, W. E. & Pentcheva, R. Massive Symmetry Breaking in $LaAlO_3/SrTiO_3$(111) Quantum Wells: A Three-Orbital Strongly Correlated Generalization of Graphene. *Phys. Rev. Lett.* **111**, 126804 (2013).
28. Blaha, P., Schwarz, K., Madsen, G. K. H., Kvasnicka, D. & Luitz, J. *WIEN2k, An Augmented Plane Wave Plus Local Orbitals Program for Calculating Crystal Properties* ISBN 3-9501031-1-2 (Vienna University of Technology, Vienna, Austria, 2001).
29. Perdew, J. P., Burke, K. & Ernzerhof, M. Generalized Gradient Approximation Made Simple. *Phys. Rev. Lett.* **77**, 3865–3868 (1996).
30. Anisimov, V. I., Zaanen, J. & Andersen, O. K. Band theory and Mott insulators: Hubbard U instead of Stoner I. *Phys. Rev. B* **44**, 943–954 (1991).
31. Solovyev, I., Hamada, N. & Terakura, K. t_{2g} versus all 3*d* localization in La*M*O_3 perovskites (*M* = TiCu): First-principles study. *Phys. Rev. B* **53**, 7158–7170 (1996).
32. Pavarini, E. *et al.* Mott Transition and Suppression of Orbital Fluctuations in Orthorhombic $3d^1$ Perovskites. *Phys. Rev. Lett.* **92**, 176403 (2004).
33. Streltsov, S. V. *et al.* Crystal-field splitting for low symmetry systems in ab initio calculations. *Phys. Rev. B* **71**, 245114 (2005).
34. Kokalj, A. Computer graphics and graphical user interfaces as tools in simulations of matter at the atomic scale. *Comp. Mater. Sci.* **28**, 155–168 (2003).
35. Bjaalie, L., Janotti, A., Himmetoglu, B. & Van, C.G. Turning $SrTiO_3$ into a Mott insulator. *Phys. Rev. B* **90**, 195117 (2014).

Acknowledgments

R.P. and D.D. acknowledge discussions with W.E. Pickett, S. Stemmer, Ariando, M.S. Golden and A. Janotti, as well as financial support through the DFG SFB/TR80 (project C3/G3).

Author contributions

D.D. performed the calculations under the guidance of R.P., D.D. and R.P. analyzed and interpreted the results and wrote the manuscript.

Additional information

Competing financial interests: The authors declare no competing financial interests.

How to cite this article: Doennig, D. & Pentcheva, R. Control of orbital reconstruction in $(LaAlO_3)_M/(SrTiO_3)_N(001)$ quantum wells by strain and confinement. *Sci. Rep.* **5**, 7909; DOI:10.1038/srep07909 (2015).